

Provided for non-commercial research and education use.  
Not for reproduction, distribution or commercial use.



This article was published in an Elsevier journal. The attached copy is furnished to the author for non-commercial research and education use, including for instruction at the author's institution, sharing with colleagues and providing to institution administration.

Other uses, including reproduction and distribution, or selling or licensing copies, or posting to personal, institutional or third party websites are prohibited.

In most cases authors are permitted to post their version of the article (e.g. in Word or Tex form) to their personal website or institutional repository. Authors requiring further information regarding Elsevier's archiving and manuscript policies are encouraged to visit:

<http://www.elsevier.com/copyright>



# Modelling of microsegregation and homogenization of 6061 extrudable Al-alloy

S.N. Samaras, G.N. Haidemenopoulos\*

Laboratory of Materials, Department of Mechanical and Industrial Engineering, University of Thessaly, Pedion Areos, 38334 Volos, Greece

Received 7 March 2006; received in revised form 28 March 2007; accepted 30 March 2007

## Abstract

A simulation of the evolution of the as-cast microstructure during the homogenization heat treatment of A6061 aluminum alloy is presented. The microstructure is dendritic with phase and solute segregation. The alloy microsegregation, which results after casting, was calculated with the Scheil equation by employing computational alloy thermodynamics. The microstructure evolution during homogenization was simulated by employing computational kinetics for the solution of the multicomponent diffusion equations. The composition profiles of the alloying elements and the volume fraction of the secondary phases were calculated as a function of homogenization time. The simulation results were validated qualitatively by comparison with metallographic examinations. During homogenization, the  $Mg_2Si$  dissolution and the transformations of the Fe-intermetallics were confirmed. It is concluded that the model reproduces the homogenization kinetics reasonably and it is capable for the prediction of the homogenization heat treatment completion times.

© 2007 Elsevier B.V. All rights reserved.

*Keywords:* Continuous casting; Intermetallics; Microsegregation; Homogenization; Simulation

## 1. Introduction

Large-scale ingots, suitable for forming processes, such as extrusion and rolling, are produced with the direct-chill casting method. The majority of the extrudable 6XXX aluminum alloy series are produced with this method. The 6XXX aluminum alloys, which are based on the ternary Al–Mg–Si alloy system, contain 1.5% Mg and Si with a ratio 1.73:1 for the formation of the  $Mg_2Si$  phase [1]. Depending on the desirable mechanical properties, the Mg and Si chemical composition of these alloys may vary according to Fig. 1 [2]. Other elements, such as Mn, Zn and Cr are used as recrystallization inhibitors and for grain size control at the subsequent forming processes [3]. In commercial alloys containing Al–Mg–Si–Fe–Mn–Cu–Cr–Zn several phases may be present. Besides the  $Mg_2Si$  phase, which contributes to the final mechanical properties, Fe in combination with Si may form the ternary phases  $\alpha$ -AlFeSi,  $\beta$ -AlFeSi or else with Cr, Mn the quaternary phase  $\alpha$ -Al(MnCrFe)Si [4]. The solidification path of these alloys is quite complex and consists of binary, ternary and even more quaternary eutectic reactions [5,6]. A list

of the primary reactions observed during the solidification of these alloys is given in Table 1.

The as-cast material possesses low formability due to the following microstructure inhomogeneities [3]:

- Microsegregation, grain boundary segregation, low melting point eutectics and brittle intermetallic compounds.
- Supersaturated solutions of finely dispersed precipitates of the alloying components (e.g.  $Al_6Mn$ , AlFeMn,  $Mg_2Si$ , AlFeSi,  $Al_{13}Fe_4$ ) increase the high temperature flow stress.
- Certain alloying elements, including manganese, iron and zirconium, either in solid solution or as finely dispersed precipitates, retard recrystallization. This effect is of particular significance in the extrusion of AlMgSi(Mn) alloys for color anodization and also if the extrusion effect (recrystallization inhibition) is to be utilized.

These effects can be partly or completely eliminated by the homogenization heat treatment of the cast billets. The main benefits of this process are the following [7]:

- Removal of microsegregation.
- Removal of non-equilibrium low melting point eutectics, particles and segregation gradients that will give areas with low

\* Corresponding author. Tel.: +30 24210 74061; fax: +30 24210 74062.  
 E-mail address: hgreg@mie.uth.gr (G.N. Haidemenopoulos).

**Nomenclature**

- $c_i$  concentration of element  $i$
- $c_i^e$  equilibrium concentration of element  $i$
- $C_0$  the alloy nominal composition
- $C_m$  minimum concentration of element  $i$  at time  $t$
- $C_M$  maximum concentration of element  $i$  at time  $t$
- $C_s$  the element composition of the last solidified solid when the solid weight fraction is  $f_s$
- $C_m^0$  minimum initial concentration of element  $i$
- $C_M^0$  maximum initial concentration of element  $i$
- $D$  diffusivity in the matrix
- $D_{eff}$  effective diffusivity
- $D_p$  diffusivity in the particles
- $D_{ij}^n$  diffusion coefficient of element  $i$  due to concentration gradient of element  $j$
- $f_s$  weight fraction of solid
- $i$  Mg, Si, Fe, Mn
- $J_i$  diffusion flux of element  $i$
- $K$  the partition coefficient
- $L$  length of dendrite arms

*Greek symbols*

- $\delta_i$  microsegregation index of element  $i$
- $\phi_p$  volume fraction of dispersed particles
- $\phi_s$  volume fraction of solid

Table 1

Invariant solidification reactions

Invariant reaction	Reference
$L \rightarrow Al + Mg_2Si$	[1]
$L \rightarrow Al_{13}Fe_4 + \alpha-Al$	[21,22]
$L \rightarrow Al_{13}Fe_4 \rightarrow \alpha-AlFeSi + \alpha-Al$	[21]
$L \rightarrow \alpha-AlFeSi + \alpha-Al$	[21,22]
$L + \alpha-AlFeSi \rightarrow \beta-AlFeSi + \alpha-Al$	[21]
$L \rightarrow \beta-AlFeSi + \alpha-Al$	[22]
$L \rightarrow \beta-AlFeSi + \alpha-Al + Si$	[22]
$L \rightarrow \beta-AlFeSi + Mg_2Si + \alpha-Al$	[9,21]
$L \rightarrow \alpha-Al(FeMn)Si + Mg_2Si + \alpha-Al + Si$	[21]

cooling. When the heating starts at room temperature, the solid solution is strongly supersaturated. The supersaturation increases from the center to the edge of the dendrite arms due to microsegregation. The first transformation, which takes place is nucleation and growth of Fe, Mn and  $Mg_2Si$  precipitates, which redissolve at higher temperatures. During the holding time, homogenization of concentration gradients takes place on the dendrite arm spacing scale. This homogenization decreases the concentration to areas with high precipitate volume fractions, mostly at the edge of dendrite arms. This leads to dissolution of particles, which have formed during the previous (heating) step. Other major reactions during this step involve coarsening of dispersoids, spheroidization of undissolved particles and the transformation  $\beta-AlFeSi \rightarrow \alpha-AlFeSi$ , which is important due to the low high temperature ductility of the  $\beta$ -phase [8,9].

A high temperature below the melting point is selected for homogenization in order to reduce process time. Local melting can cause severe damage at the alloy microstructure inducing voids, cracks and blistering during extrusion [10]. Segregated regions can be melted at lower temperatures from the liquidus. Consequently, a safe limit for the homogenization temperature should be the eutectic temperature for the  $Mg_2Si$  invariant reaction.

At the cooling step re-precipitation of particles, which were dissolved at the previous steps, occurs. The final size of the  $Mg_2Si$  and Fe, Mn, Cr particles is significant for recrystallization [8] or grain size control during subsequent hot working and improvement of final mechanical properties [3]. For the above arguments and in order to be able to dissolve during hot working, the particle dispersion should be fine. The particle size should be large for reduced solid solution strengthening during hot working (high extrudability) [11], but not too high for enhanced dissolution during extrusion (small solutionizing times) [8,12].

During the last decades several research efforts focused on aluminum extrusion processing. The objective of these studies has been the correlation between microstructure and process conditions for enhanced extrudability. For the 6XXX aluminum alloy series, the study of the  $Mg_2Si$  dispersion and the Fe-intermetallics transformations is a crucial feature. Several authors studied the influence of the cooling rate after homogenization on the alloy microstructure. Zajac et al. [13] and Nowotnik and Sieniawski [14] studied the influence of the cool-

- melting point in order to avoid cracking or tearing during subsequent hot working.
- c. Shape control (round-off) of hard particles with sharp edges, such as Fe-based intermetallics, which give poor ductility.
- d. Formation of secondary particles (dispersoids) for grain size control during extrusion or rolling.
- e. Uniform distribution of alloying elements in solid solution before extrusion or rolling and age hardening.

Industrial homogenization for aluminum alloys is a three-step process with heating, holding to high temperature and

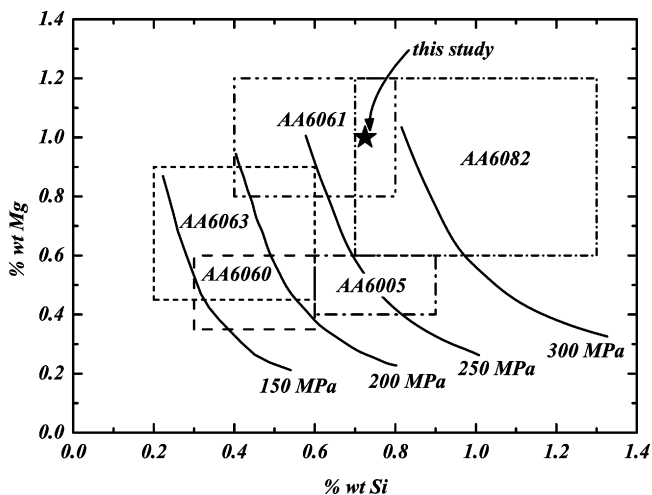


Fig. 1. Composition limits of 6XXX AA [1].

ing rate on the final mechanical properties for the 6063, 6082, 6005 alloys. Reiso [15] studied the influence of the cooling rate on the extrusion speed for various chemical compositions of AlMgSi alloys. Birol [12] studied the microstructure evolution of the 6063 alloy during homogenization for various thermal cycles. Cai et al. [16] studied the Mg<sub>2</sub>Si dissolution during homogenization through electrical resistivity measurements and the distribution of the alloying elements with electron microprobe measurements for the 6061, 6069 alloys. Finally, Usta et al. [17] and van de Langkruis [11] studied the dissolution/coarsening kinetics of the Mg<sub>2</sub>Si particles during reheating of the homogenized material.

The present work emphasizes on the simulation of the microstructure evolution during the holding period of the homogenization of the 6061 aluminum alloys. The evolution of the as-cast microstructure was examined with standard metallographic techniques. The microsegregation of the as-cast microstructure was calculated by applying computational thermodynamics techniques, more specifically the ThermoCalc software. From the metallographies a geometric model was defined for the solution of the diffusion equation. The kinetic model was solved with the computational kinetics DICTRA software. The results obtained include the volume fraction of secondary phases and the concentration profile of the alloying elements. The model results were validated qualitatively by comparison with the metallographic examinations. It will be shown that the model can reproduce the homogenization kinetics reasonably and it is capable to predict the completion time for the Mg<sub>2</sub>Si dissolution and the microsegregation removal during the homogenization heat treatment of 6XXX aluminum alloys.

## 2. Experimental

The aluminum alloy used in the present investigation was cast industrially with a vertical dc caster, in the form of 4 m long billets with a diameter of 20 cm. A total of 10 t material was cast producing 22 billets. The liquid metal temperature in the mold was 680–695 °C and the casting speed 90 mm/min. The chemical composition of the alloy is given in Table 2 and follows the 6061 specification for the Si, Fe, Mn, Mg but not for the Cu, Cr, Zn.

Homogenization trials were performed at 580 °C with a soak time from 0 to 8 h. Samples for homogenization were sectioned from a transverse slice of the billet, at the middle of the billet radius, in order to avoid possible microstructural and compositional variations near the billet surface. The homogenized samples were water-quenched and prepared with standard metallographic techniques; they were ground with SiC paper and polished with Al<sub>2</sub>O<sub>3</sub> suspension. They were etched with a 0.5% HF solution for 4–5 s in order to enhance the contrast between Mg<sub>2</sub>Si (black) and Fe-phases (gray) at the grain boundaries [9,18]. Some of the samples were slightly over-etched to facilitate direct observation of fine particles with the light microscope. Dark field images were also taken for resolution improvement [12]. Finally, images were taken at different homogenization times for the examination of the microstructure evolution and the subsequent correlation with the simulation results.

Table 2  
Chemical composition

	Si	Fe	Cu	Mn	Mg	Cr	Zn
Alloy	0.725	0.315	0.038	0.114	1	0.002	0.034
AA6061	0.4–0.8	0–0.7	0.15–0.4	0–0.15	0.8–1.2	0.04–0.35	0–0.25

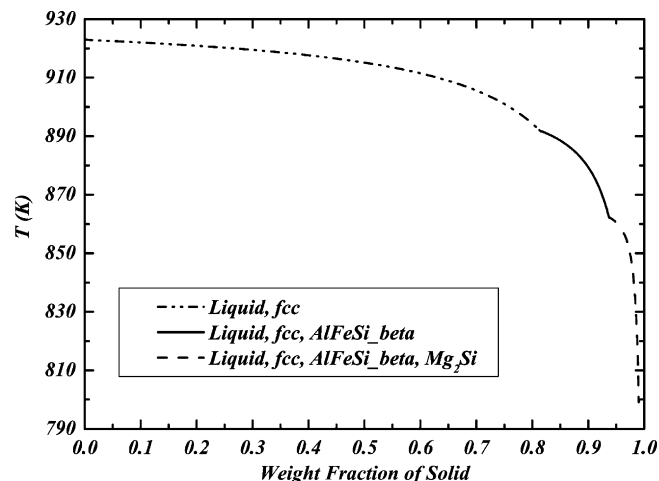


Fig. 2. Solidification path of the studied alloy.

## 3. Results

### 3.1. Solidification path—microsegregation

Microsegregation in aluminum is a result of the low solubility of the alloying elements in the solid in relation with the liquid. The low aluminum solid solubility leads to the formation of secondary phases in the as-cast microstructure. The size and morphology of these phases depends on the chemical composition, the dendrite arm spacing, the grain size and the local solidification time. Assuming negligible diffusion in the solid state during casting, the composition profile of the alloying elements can be described with the Scheil equation:

$$C_s = C_0 K (1 - f_s)^{K-1} \quad (1)$$

where  $C_0$  is the alloy nominal composition,  $K$  the partition coefficient and  $C_s$  is the element composition of the last solidified solid when the solid weight fraction is  $f_s$ . The Scheil calculations for a multicomponent alloy system can be performed with the CALPHAD method and specifically with the THERMOCALC software [19].

In Fig. 2, the alloy solidification path is calculated according to Scheil equation. The assumption of negligible diffusion in the solid is acceptable due to the short local solidification time at industrial direct-chill casting conditions. The phases included in the Scheil calculations were the Mg<sub>2</sub>Si and  $\beta$ -AlFeSi. Other phases, such as  $\alpha$ -AlFeSi and Al<sub>13</sub>Fe<sub>4</sub> that might exist at equilibrium conditions, were not included in the calculations since it was considered that the  $\beta$ -AlFeSi phase is dominant in the 6XXX alloy microstructure [20]. This situation is true for high solidification rates, up to 30 mm/min [18,21] and when AlTiB grain refiners are used [22].

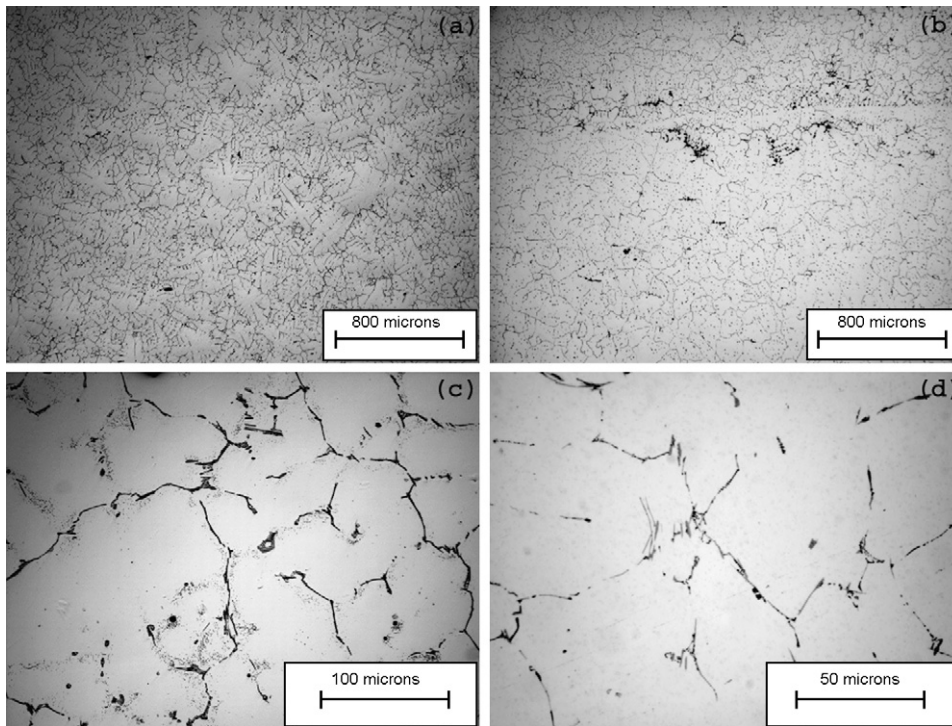


Fig. 3. The as-cast microstructure of the studied alloy: (a) X50, typical dendritic microstructure, (b) X50 chill zone at the billet edge, (c) X500 phase morphology at the dendrite arms, fine  $Mg_2Si$  particles and (d) X1000 black  $Mg_2Si$  and gray  $\beta-AlFeSi$  particles.

The as-cast microstructure is shown in Fig. 3. Fig. 3a shows a typical dendritic microstructure. Fig. 3b, which corresponds to the billet edge, shows the existence of the chill zone and the grain refinement due to the high temperature gradients during casting. At high magnification, in Fig. 3d, after 4–5 s etching with 0.5% HF, the morphology of black  $Mg_2Si$  and gray  $\beta-AlFeSi$  is revealed. Similar over etched samples in Fig. 3c show a fine distribution of  $Mg_2Si$  particles near the grain boundaries.

The predicted concentration of the alloying elements in the aluminum matrix (FCC) and in the liquid as a function of the fraction of solidified solid is given in Fig. 4. The fraction of the secondary phases also is given. It can be seen that the simulation correctly predicts the increasing concentration of the alloying elements as solidification proceeds. The fall in the Mg, Si and Fe concentration predicted in the matrix close to the end of the solidification coincides with the point where the  $Mg_2Si$  and  $\beta-AlFeSi$  phases start to form.

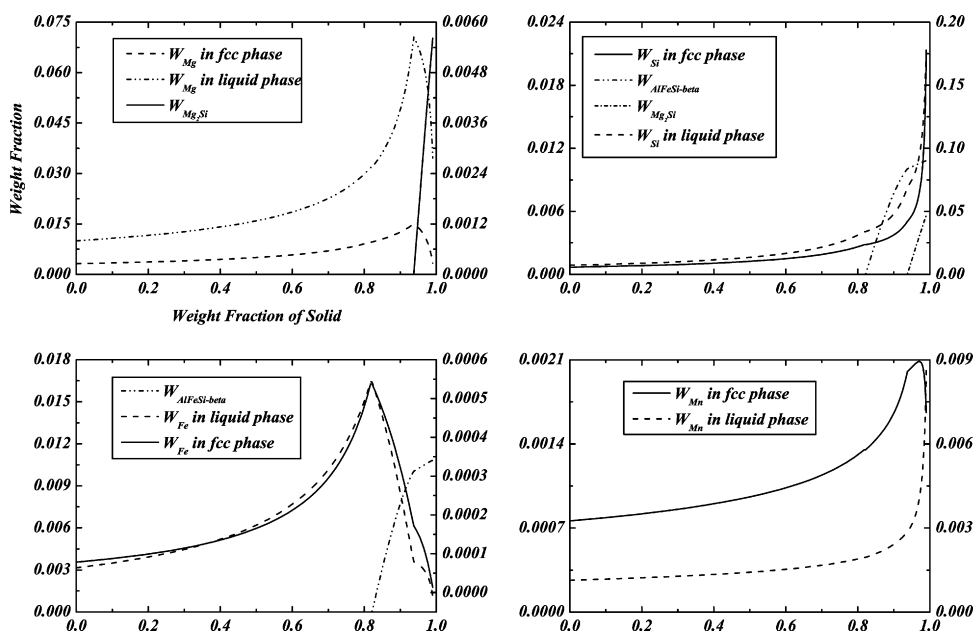


Fig. 4. Microsegregation–concentration profiles of the alloying elements.

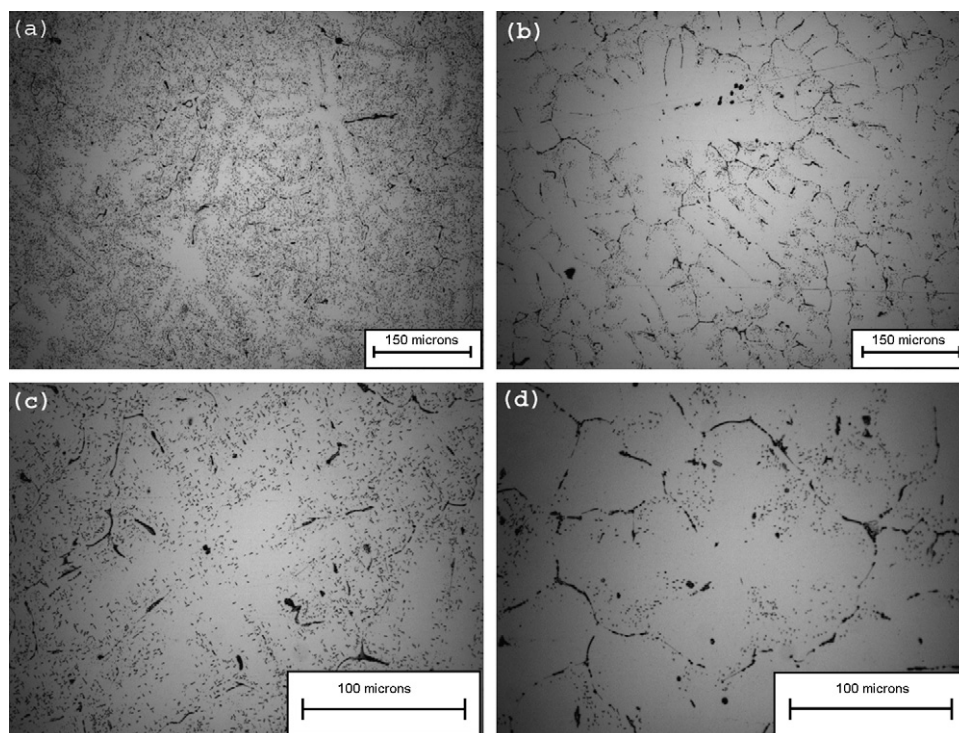


Fig. 5. Precipitation in segregated regions: (a) X200,  $T=400\text{ }^{\circ}\text{C}$ , (b) X200,  $T=500\text{ }^{\circ}\text{C}$ , (c) X500,  $T=400\text{ }^{\circ}\text{C}$  and (d) X500,  $T=500\text{ }^{\circ}\text{C}$ .

The calculated concentration profiles can be correlated with a characteristic length of the microstructure. A usual practice in the literature is to correlate these profiles either with the dendrite arm spacing [23,24] or with the grain size [16]. However, the dendrite/grain growth is two-dimensional and the profiles should be described with iso-concentration contours. In order to observe the solute distribution within the grains, as-cast samples were heat treated at two temperatures 400 and 500 °C for 15 min. In supersaturated grain regions, secondary precipitation occurs. The temperature selection was based on the following conditions. First, the particle dispersion should be observable and second to avoid supersaturation of the whole grain. Therefore, the temperature should be over 300 °C, where high particle growth occurs and the supersaturation is relatively low. The heat-treated material is shown in Fig. 5. A second-phase precipitation is observed perimetric to the dendrite arms confirming the two-dimensional distribution of the microsegregation. The precipitate regions are the last to solidify and possess the highest supersaturation. The difference in precipitate zone length difference is related with the concentration difference. This is because solid solubility increases with increasing temperature, causing a decrease of the precipitate zone length.

### 3.2. Metallographic examination of microstructure evolution during homogenization

The microstructure evolution during homogenization was examined with standard optical microscopy techniques. Samples were taken from the middle of the billet radius in order to avoid edge inhomogeneities. The samples were heat treated at 580 °C for various times. The microstructure is shown in Figs. 6 and 7

after 5 and 30 s etching with 0.5% HF at bright and dark field, respectively.

In Fig. 6a the morphology of the black  $\text{Mg}_2\text{Si}$  and gray  $\beta\text{-AlFeSi}$  phases is shown. The  $\beta\text{-AlFeSi}$  phase is located at the dendrite arms edge in plate form. The  $\text{Mg}_2\text{Si}$  phase is in the form of spherical or plate-like particles attached to the  $\beta\text{-AlFeSi}$  plates. For longer times,  $\text{Mg}_2\text{Si}$  dissolution takes place (Fig. 6b and c). Simultaneously, heterogeneous nucleation and growth of the  $\alpha\text{-AlFeSi}$  on the  $\beta\text{-AlFeSi}$  plates occurs, rounding-off the Fe-intermetallics (Fig. 6d–f) [9]. The  $\text{Mg}_2\text{Si}$  dissolution is completed after 2 h, while the  $\beta \rightarrow \alpha$  transformation is completed after 68 h. These times are in good agreement with relevant literature data [9,16]. The  $\alpha\text{-AlFeSi}$  and  $\beta\text{-AlFeSi}$  can be distinguished through their shape, since they appear as particles with round and sharp edges, respectively.

The microstructure of overetched samples in dark field is shown in Fig. 7. The additional information here is the existence of a fine dispersion near the dendrite arm edges. This dispersion consists of  $\text{Mg}_2\text{Si}$  and  $\alpha\text{-AlFeSi}$  [9,12] particles, which at longer times coarsen and dissolve due to removal of microsegregation. This dissolution/coarsening effect decreases the particle density, which is shown in Fig. 7. These observations are confirmed in Fig. 8, where for long time heat treatment, the resulting microstructure consists of a fully coarsened dispersion with rounded Fe-intermetallics at the grain boundaries.

### 3.3. Simulation of the microstructure evolution

The homogenization heat treatment can be simulated as a diffusion-precipitation process. The following phenomena take place simultaneously: (a) precipitation close to the dendrite arm

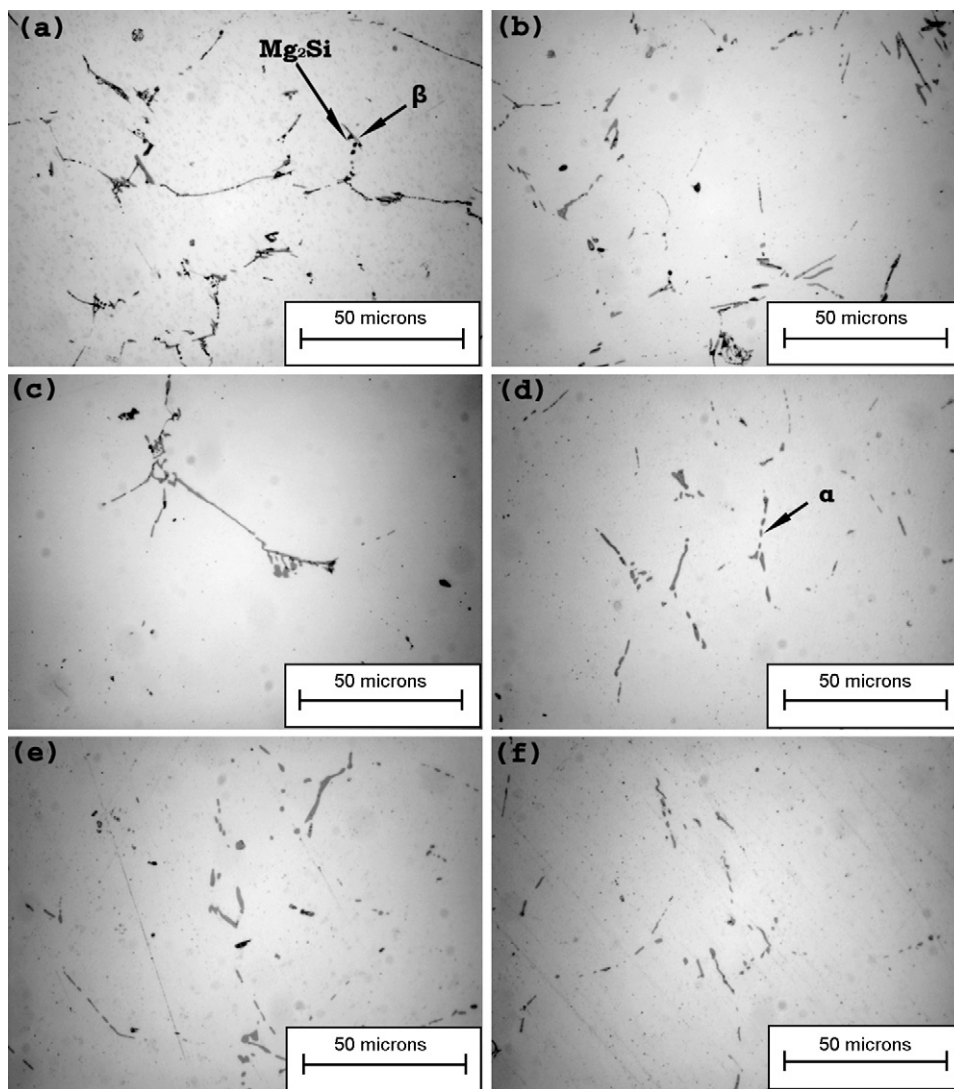


Fig. 6. Microstructure evolution during homogenization at 580 °C, X1000, 0.5% HF reagent, etching time 5 s, bright field: (a) as-cast, (b) 40 min, (c) 2 h, (d) 4 h, (e) 8 h and (f) 10 h.

boundaries, (b) removal of microsegregation, (c) precipitation inside the grains and (d) phase dissolution. Bulk diffusion or precipitation/dissolution reactions control the overall kinetics [25], depending on the temperature and the diffusion length. For the complete definition of the as-cast microstructure the following information is needed:

- Initial concentration profiles of the alloying elements.
- Secondary phases volume fraction.
- Secondary phases morphology within the grains.
- Thermal cycle.
- A geometric model where the diffusion equations will be solved.

The initial concentration profiles and the volume fraction of secondary phases are the results from the Scheil calculations (Fig. 4). The thermal cycle is an operational parameter having as an upper limit the eutectic temperature. The dissolution temperatures of the second phases are given in Table 3. The second

phases consists of (a) fine  $Mg_2Si$  particles attached to the  $\beta$ -AlFeSi plates (Figs. 6 and 7) and (b) a fine dispersion of  $Mg_2Si$  particles near the dendrite arm boundaries (Fig. 3c). An appropriate geometric model should include the above considerations and physical mechanisms. To that end, the geometry of Fig. 9 was considered for the description of the homogenization heat treatment.

In the model of Fig. 9, two regions are considered, with matrix phases the FCC and  $\beta$ -AlFeSi, respectively. In the FCC phase,

Table 3  
Dissolution temperatures of phases for the AA6061 (calculated with ThermoCalc) [19]

Phase	Temperature (K)	
$\alpha$ -AlFeSi	901.74	
$\beta$ -AlFeSi	873.19	
$Mg_2Si$	833.94	
FCC	922.97	Liquidus
$\Upsilon\gamma\delta$	870.84	Solidus

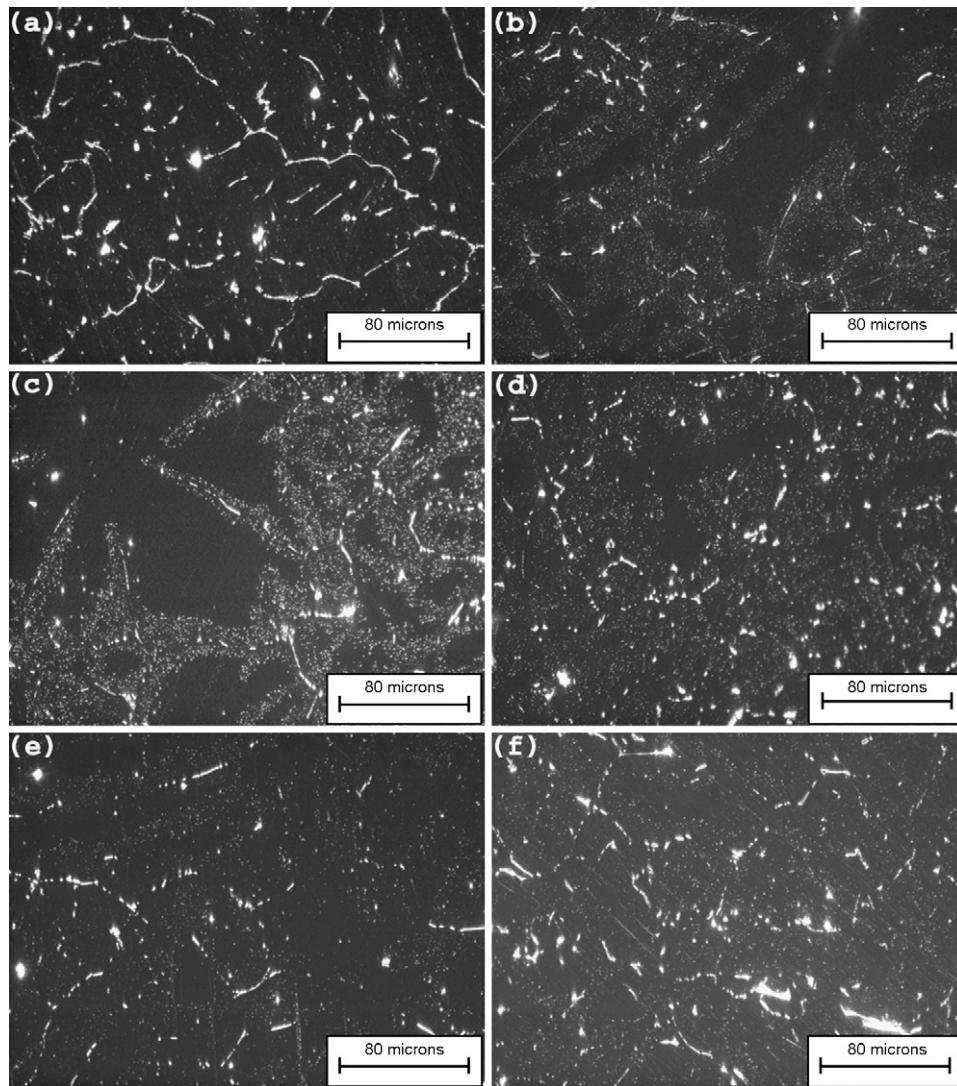


Fig. 7. Microstructure evolution during homogenization at 580 °C, X1000, 0.5% HF reagent, etching time 30 s, dark field: (a) as-cast, (b) 40 min, (c) 2 h, (d) 4 h, (e) 8 h and (f) 10 h.

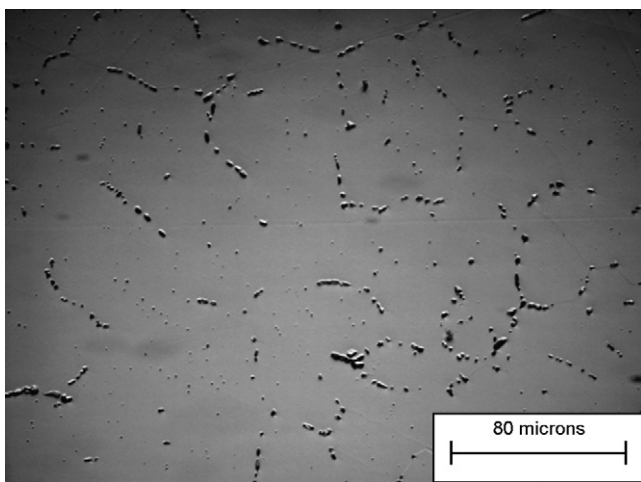


Fig. 8. Alloy microstructure after 3 days heat treatment at 580 °C, X500, Kellers reagent, etching time 30 s.

the  $Mg_2Si$  and  $\alpha-AlFeSi$  are allowed to be in dispersion. This diffusion problem was solved with the computational kinetics package DICTRA [19]. The DICTRA module for diffusion in dispersed systems treats problems involving diffusion through microstructures containing dispersed precipitates of secondary phases. Diffusion is assumed to take place only in the matrix phase. The dispersed phases act as point sinks or sources of solute atoms in the simulation and their fraction and composition is calculated from the average composition in each node, assuming that equilibrium holds locally in each volume element. The calculation scheme consists of two steps. The first step is the so-called diffusion step, which is simply a one-phase problem since it is assumed that all diffusion occurs in a matrix phase. However, due to the composition change in the matrix during the diffusion step, there is a change in the average composition at every node. The new equilibrium is calculated from the new average composition using ThermoCalc, and the diffusion step is then repeated with the new composition profile in the matrix phase, and so on. This module is suitable for long-range diffusion cal-

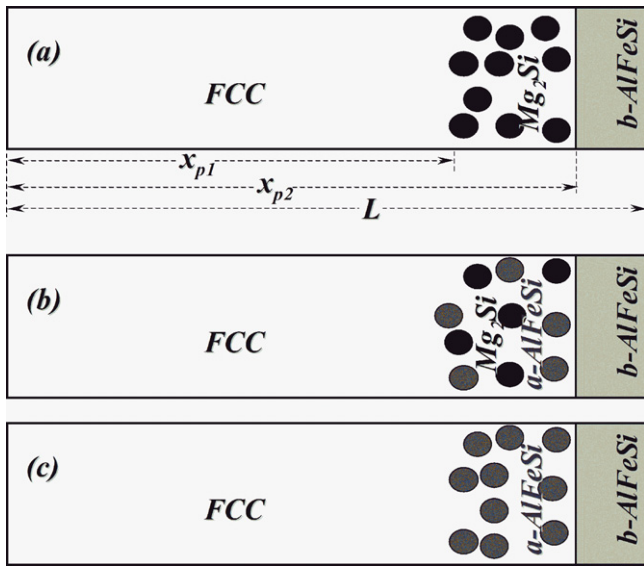


Fig. 9. (a–c) Geometric model for the simulation of the homogenization heat treatment.

culations compared with the inter-particle distances. The basic model assumption is that the growth and dissolution rates are very high compared with the diffusion rates in the matrix. Alternatively, the matrix diffusion is the controlling mechanism of the overall kinetics. This assumption is tolerable for the high homogenization temperatures, since the growth-dissolution rates are very high and the particles reach the equilibrium state very fast. Consequently the local conditions are rather concentration-dependent than time-dependent. Locally, most of the solute is trapped into the particles, reducing the concentration gradients and the diffusion rate in the matrix. In the case of low temperature or low diffusion coefficients, the diffusion in the matrix should be solved implicitly with a time-dependent precipitation model [25].

Although the microstructure geometry is two-dimensional, as discussed before, the Fick second law is solved in one dimension. The length of dendrite arms is five to six times their width. The diffusion fluxes are calculated from the Onsager–Fick law for multicomponent systems with concentration-dependent diffusion coefficients:

$$\frac{\partial c_i}{\partial t} = \frac{\partial J_i}{\partial x} \quad (2)$$

$$J_i = - \sum_{j=1}^{n-1} D_{ij}^n \frac{\partial c_j}{\partial x} \quad (3)$$

The diffusion flux through the FCC matrix is reduced due to the existence of precipitates. The diffusion coefficients are replaced with equivalent effective diffusivities, which depend on the precipitate volume fraction [26]:

$$\frac{D_{\text{eff}}}{D} = \frac{2/D_s + 1/D - 2\phi_p(1/D_s - 1/D)}{2/D_s + 1/D + \phi_p(1/D_s - 1/D)} \quad (4)$$

where  $D$  is the diffusivity in the matrix,  $D_p$  the diffusivity in the particles and  $\phi_p$  is the particle volume fraction. Eq. (4) has two asymptotic cases, when the diffusion through the par-

ticles is much higher or lower compared with the diffusion in the matrix. Mathematically, this is expressed as  $D_p \rightarrow \infty$  and  $D_p \rightarrow 0$ , respectively, resulting to the following relations:

$$\frac{D_{\text{eff}}}{D} = \frac{1 + 2\phi_p}{1 - \phi_p} \quad (5)$$

$$\frac{D_{\text{eff}}}{D} = \frac{2(1 - \phi_p)}{2 + \phi_p} \quad (6)$$

Eq. (6) will be used in the present case.

Defining, zero flux conditions through the grain boundaries, the boundary conditions are:

$$\left. \frac{\partial c_i}{\partial x} \right|_{x=0} = 0 \quad (7)$$

$$\left. \frac{\partial c_i}{\partial x} \right|_{x=L} = 0, \quad i = \text{Mg, Mn} \quad \text{and} \quad c_i(L, t) = c_i^e, \quad i = \text{Fe, Si} \quad (8)$$

The initial conditions for solving the diffusion problem are the results of the Scheil calculations. The following relation can be used in order to correlate the solid phase volume fraction with the diffusion distance:

$$\phi_s = \frac{x}{L} \quad (9)$$

Using Eq. (9) the concentration profiles from the Scheil calculations in Fig. 4 can be converted over the diffusion distance. The local volume fraction of the dispersed phase is calculated from the following relation (a simple mass balance using Eq. (9)):

$$\phi'_{p,j} = \phi_p \frac{L - x_{p1}}{L} \quad (10)$$

The model results are the evolution of the concentration profiles of the alloying elements, the variation of the volume fraction of secondary phases and the total volume fraction of the secondary phases.

The evolution of the concentration profiles of the alloying elements is shown in Fig. 10. At short times, precipitation takes place at the dendrite arm boundaries, due to the high supersaturation. This result is consistent with the microstructure photos in Fig. 7. The concentration reduction is due to phase precipitation and not due to diffusion in the matrix. The high Mg and Si diffusion coefficients smooth over the concentration profiles quickly and lead to dissolution of the  $\text{Mg}_2\text{Si}$  particles due to the solute depletion of the supersaturated regions. The diffusion of Fe and Mn is very slow. The  $\alpha\text{-AlFeSi}$ ,  $\beta\text{-AlFeSi}$  phases are partly undissolvable (as predicted from the phase diagram) at the grain boundaries. The dispersion of Fe-intermetallics undergoes coarsening gradually with time (Fig. 7). In Fig. 8 a fully coarsened dispersion is observed after 3 days heat treatment. Possible Mn particles are undissolvable at the grain boundaries due to the negligible Mn diffusion. These particles retard recrystallization in subsequent thermomechanical processes.

The evolution of the volume fraction profiles of the secondary phases is shown in Fig. 11. The initial  $\text{Mg}_2\text{Si}$  precipitation at

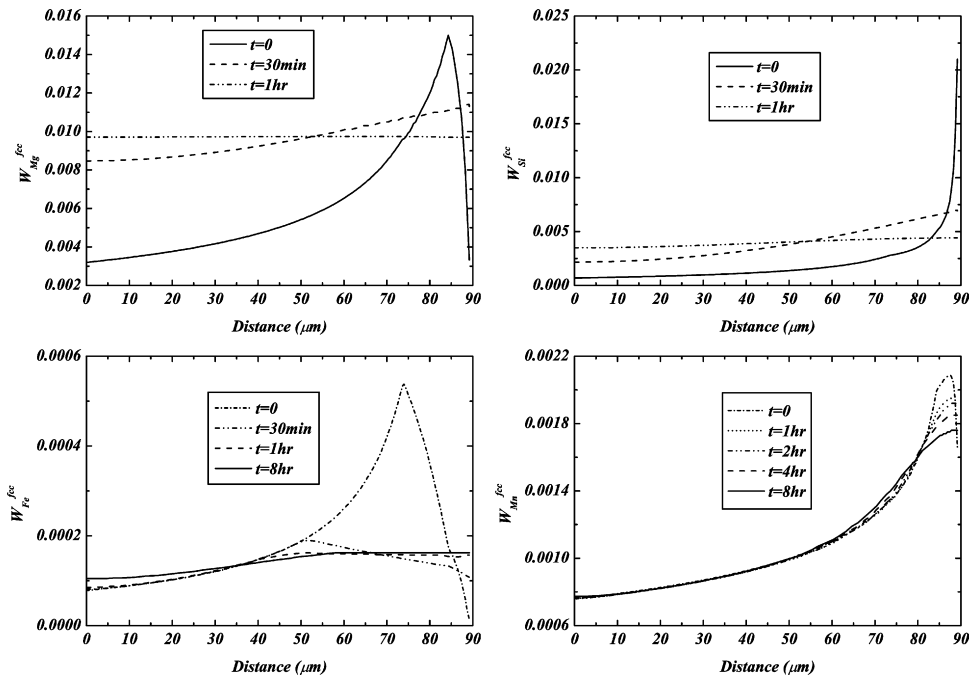


Fig. 10. Evolution of the alloying elements composition profiles during homogenization at 580 °C.

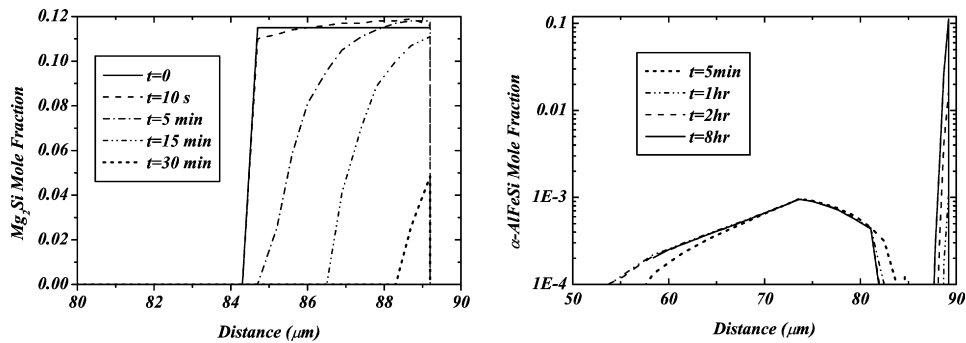


Fig. 11. Evolution of the secondary phases mole fraction profiles during homogenization at 580 °C.

the supersaturated regions and the subsequent dissolution due to solute depletion near the grain boundaries is shown. The  $Mg_2Si$  dissolusion rates are given in Fig. 12, where an increase in dissolusion rate is predicted with increasing temperature and decreasing diffusion length.

For the quantification of the evolution of microsegregation the following index is used [24]:

$$\delta_i = \frac{C_M - C_m}{C_M^0 - C_m^0} \quad (11)$$

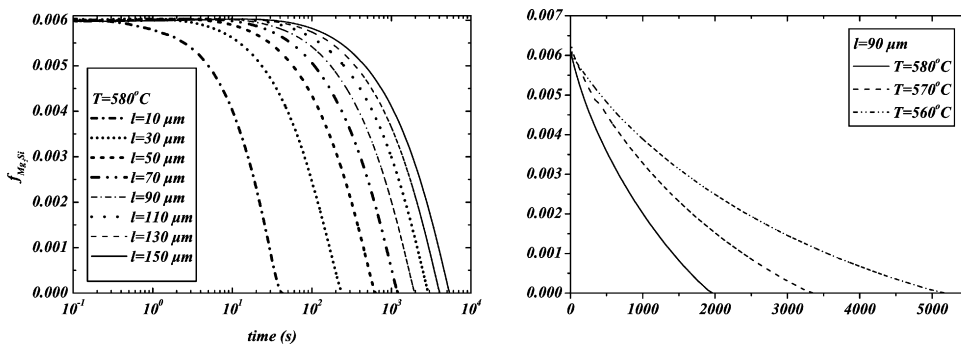


Fig. 12. Evolution of  $Mg_2Si$  volume fraction.

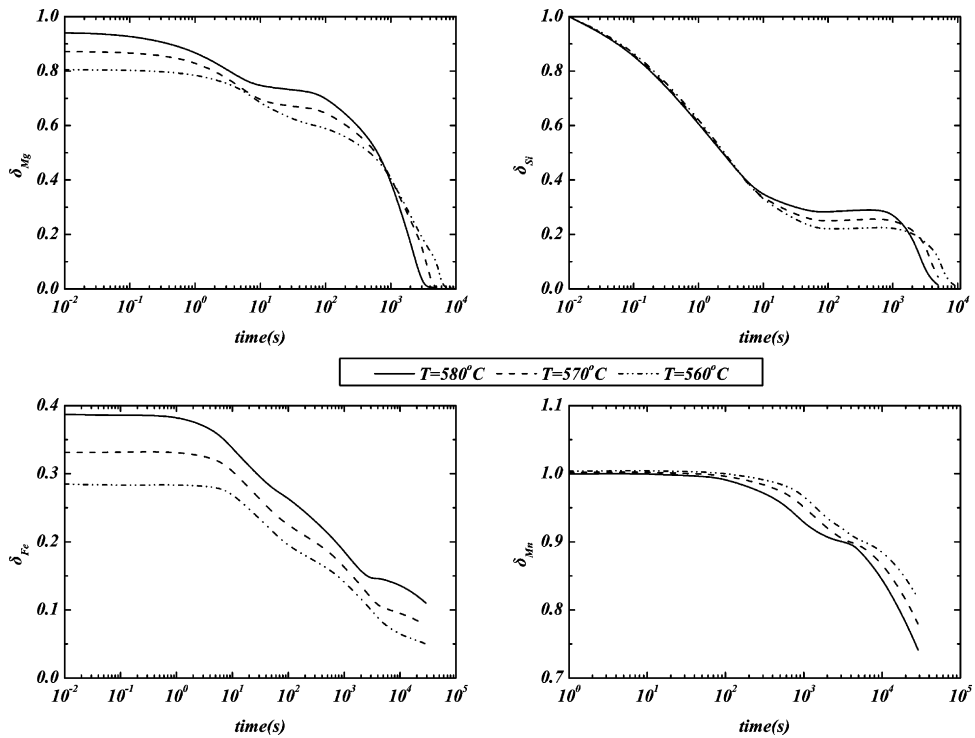


Fig. 13. Evolution of the microsegregation index for  $l = 90 \mu\text{m}$  at various temperatures.

where  $C_M$  is the maximum concentration of element  $i$  at time  $t$ ,  $C_m$  the minimum concentration of element  $i$  at time  $t$ ,  $C_M^0$  the maximum initial concentration of element  $i$ ,  $C_m^0$  the minimum initial concentration of element  $i$ ,  $\delta_i$  the microsegregation index of element  $i$  and  $i = \text{Mg, Si, Fe, Mn}$ .

At the initial time  $t = 0$ , the index  $\delta = 1$ , while after full homogenization  $\delta = 0$ . In Figs. 13 and 14 the microsegregation index versus time is given for various temperatures and grain sizes, showing the high Mg and Si homogenization rates in contrast with the low and negligible homogenization rates of Fe and Mn,

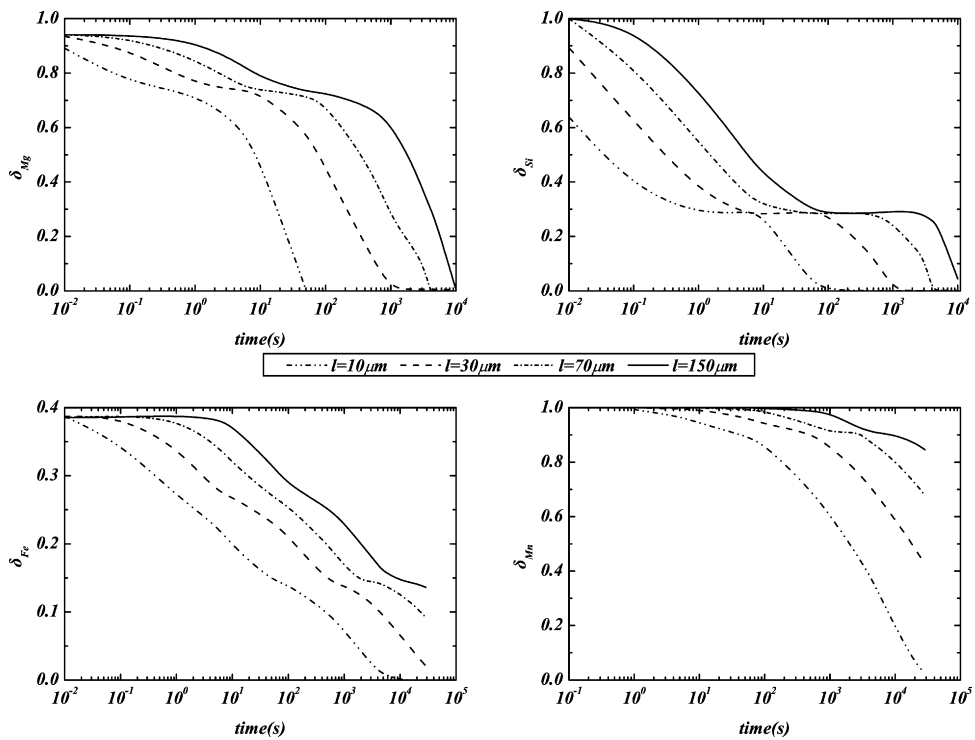


Fig. 14. Evolution of the microsegregation index for  $T = 580^\circ\text{C}$  at various diffusion lengths.

respectively. The initial value of the index  $\delta$  for Mg, Si and Fe is not equal to one, since the precipitation in the supersaturated regions reduces the maximum concentration. The microsegregation index does not follow an exponential decrease with respect to the dimensionless variable  $Dt/l^2$  [24]. A constant value appears due to the second phase dissolution (solute enrichment of the matrix phase) and then falls exponentially when the second phases reach the equilibrium value.

Summarizing, we can conclude the following:

- The model predictions are consistent with metallographic observations.
- The assumption that the dendrite length controls diffusion seems to be reasonable for the two-dimensional microsegregation distribution.
- The model estimation for the  $Mg_2Si$  dissolution time ( $\sim 2$  h for 300  $\mu m$  grain size; Fig. 12), agrees with the metallographies (2 h for  $Mg_2Si$  dissolution Fig. 6c).
- The calculation results are consistent with relevant literature references. Kuijpers [9] reported 30 min  $Mg_2Si$  dissolution time for homogenization temperature 580 °C and 4 h for the  $\beta \rightarrow \alpha$  transformation. Cai et al. [16] reported 1 h  $Mg_2Si$  dissolution time for homogenization temperature 580 °C.

#### 4. Conclusion

In the present study, the microstructure evolution during homogenization of 6XXX aluminum alloys was examined. The relevant mechanisms were the microsegregation evolution of alloying elements (Mg, Si, Mn, Fe) and the precipitation/dissolution of secondary phases ( $\beta$ -AlFeSi,  $\alpha$ -AlFeSi,  $Mg_2Si$ ) in the FCC matrix. The heat treatment was simulated as a diffusion process, taking into account the simultaneous action the diffusion of the alloying elements and the precipitation of the secondary phases. The model takes into account all the major alloying elements and secondary phases. The results were validated semi-quantitatively with standard metallographic techniques and compared with results from relevant literature studies. It is concluded that the model results are reasonable, describing satisfactory the physical mechanisms. Finally, the model is capable for the prediction of the homogenization completion times in industrial scale.

#### Acknowledgements

The present study is a part of a research project funded by the General Secretariat of Research and Technology of the Greek Ministry of Development with title 'Analysis & design of thermomechanical processes and heat treatments of aluminum alloys' in cooperation with the Hellenic Extrusion Industry EXALCO.

#### References

- [1] J.E. Hatch, Aluminum Properties and Physical Metallurgy, ASM International, 1993.
- [2] I.J. Polmear, Light alloys, in: Metallurgy of the Light Metals, Arnold, 1995.
- [3] K. Laue, H. Stenger, Extrusion: Process Machinery Tooling, ASM International, 1976.
- [4] L. Lodgaard, N. Ryum, Precipitation of dispersoids containing Mn and: or Cr in Al–Mg–Si alloys, Mater. Sci. Eng. A 283 (2000) 144–152.
- [5] Y.L. Liu, S.B. Kang, The solidification process of Al–Mg–Si alloys, J. Mater. Sci. 32 (1997) 1443–1447.
- [6] Q.G. Wang, C.J. Davidson, Solidification and precipitation behavior of Al–Si–Mg casting alloys, J. Mater. Sci. 36 (2001) 739–750.
- [7] A.L. Dons, The Alstruc homogenization model for industrial aluminum alloys, J. Light Met. 1 (2001) 133–149.
- [8] T. Sheppard, Extrusion of Aluminum Alloys, Kluwer Academic Publishers, 1999.
- [9] N.C.W. Kuijpers, Kinetics of the  $\beta$ -AlFeSi to  $\alpha$ -Al(FeMn)Si transformation in Al–Mg–Si alloys, Ph.D. Thesis, TUDelft, 2004.
- [10] P.K. Saha, Aluminum Extrusion Technology, ASM International, 2000.
- [11] J. van de Langkruis, The effect of thermal treatments on the extrusion behaviour of AlMgSi alloys, Ph.D. Thesis, TUDelft, 2000.
- [12] Y. Birol, The effect of homogenization practice on the microstructure of AA6063 billets, J. Mater. Process. Technol. 148 (2004) 250–258.
- [13] S. Zajac, B. Bengtsson, C. Jonsson, Influence of cooling after homogenization and reheating to extrusion on extrudability and final properties of AA6063 and 6082 alloys, Mater. Sci. Forum 396–402 (2002) 399–404.
- [14] G.M. Nowotnik, J. Sieniawski, Influence of heat treatment on the microstructure and mechanical properties of 6005 and 6082 aluminium alloys, J. Mater. Process. Technol. 162–163 (2005) 367–372.
- [15] O. Reiso, The Effect of Microstructure on the Extrudability of Some Aluminium Alloys, Norwegian Institute of Technology, 1992.
- [16] M. Cai, J.D. Robson, G.W. Lorimer, N.C. Parson, Simulation of the casting and homogenization of two 6xxx series alloys, Mater. Sci. Forum 396–402 (2002) 209–214.
- [17] M. Usta, M.E. Glicksman, R.N. Wright, The effect of heat treatment on  $Mg_2Si$  coarsening in aluminum 6105 alloy, Metall. Mater. Trans. A 35A (2004) 435–438.
- [18] H. Tanihata, T. Sugawara, K. Matsuda, S. Ikeno, Effect of casting and homogenizing treatment conditions on the formation of Al–Fe–Si intermetallic compounds in 6063 Al–Mg–Si alloys, J. Mater. Sci. 34 (1999) 1205–1210.
- [19] J.O. Andersson, T. Helander, L. Hoglund, P. Shi, B. Sundman, THERMOCALC & DICTRA computational tools for materials science, Calphad 26 (2002) 273–312.
- [20] S. Onurlu, A. Tekin, Effect of heat treatment on the insoluble intermetallic phases present in an AA6063 alloy, J. Mater. Sci. 29 (1994) 1652–1655.
- [21] G. Sha, K.A.Q. O'Reilly, B. Cantor, J. Worth, R. Hamerton, Growth related metastable phase selection in a 6xxx series wrought Al alloy, Mater. Sci. Eng. A 304–306 (2001) 612–616.
- [22] G. Sha, K.A.Q. O'Reilly, B. Cantor, J.M. Titchmarsh, R.G. Hamerton, Quasi-peritectic solidification reactions in 6XXX series wrought Al alloys, Acta Mater. 51 (2003) 1883–1897.
- [23] H.E. Lippard, C.E. Cambell, T. Bjorklind, U. Borggren, P. Kellgren, V.P. Dravid, G.B. Olson, Microsegregation behavior during solidification and homogenization of AerMet100 steel, Metall. Mater. Trans. B 29B (1998) 205–210.
- [24] M.C. Flemings, Solidification Processing, McGraw-Hill, 1974.
- [25] J.D. Robson, P.B. Prangnell, Modelling  $Al_3Zr$  dispersoid precipitation in multicomponent aluminium alloys, Mater. Sci. Eng. A 352 (2003) 240–250.
- [26] E.L. Cussler, Diffusion: Mass Transfer in Fluid Systems, second ed., Cambridge University Press, 1997.